Contents lists available at ScienceDirect

Chaos, Solitons and Fractals

journal homepage: http://ees.elsevier.com

Multifractal analysis of embryonic eye structures from female mice withdietary folic acid deficiency. Part I: Fractal dimension, lacunarity, divergence, and multifractal spectrum

Ouafa Sijilmassi [a,b,*], José-Manuel López Alonso [b], Aurora Del Río Sevilla [a], María del Carmen Barrio Asensio [a]

[a] Department of Anatomy and Embryology, Faculty of Optics and Optometry, Universidad Complutense de Madrid, Calle de Arcos de Jalón, 118, Madrid 28037, Spain
[b] Department of Optics, Faculty of Optics and Optometry, Universidad Complutense de Madrid, Calle de Arcos de Jalón, 118, Madrid 28037, Spain

ARTICLE INFO

Article history:
Received 14 November 2019
Received in revised form 2 May 2020
Accepted 8 May 2020
Available online xxx

Keywords
Folic acid deficiency
Collagen IV
Laminin-1
Eye structures
Multifractal analysis

ABSTRACT

The purpose of this study was to investigate effects of low maternal folic acid (FA) status on many eye structures in embryonic mice using multifractal analysis, a method for describing complex structural patterns. To do this, we used the FracLac plugin for ImageJ to analyse binary digital images of cornea, lens, retina, and vitreous after immunohistochemical analysis using anti-collagen IV or anti-laminin-1 antibodies. The box-counting and gliding box methods were used to generate metrics including the fractal dimension, lacunarity, divergence, and multifractal spectrum distance metrics for each ocular structure. Results were analysed using bootstrap resampling techniques and the Kruskal-Wallis significance test. For all structures and staining methods studied, differences between embryos from control vs FA-deficient females were detectable in lacunarity plots and multifractal spectra, and statistically significant in cornea, lens, retina and vitreous. Multifractal analysis detected even slight differences in tissue textures presumably attributable to altered expression of extracellular matrix molecules.

1. Introduction

A fractal structure is a geometric construction that has the peculiarity of being self-similar [23, 35]. Fractal analysis methods are widely used in image analysis problems in the biological and medical fields. They are used for characterizing several biological processes (e.g., morphogenesis and carcinogenesis) and biological systems (e.g., the circulatory, nervous and respiratory systems), etc. [1, 4, 20, 30, 37, 53]. In the present work, we use fractal analysis methods to evaluate changes produced in the texture of some eye structures due to maternal folic acid deficiency (FAD). It is known that folic acid (FA) is essential for the normal development of embryos. Because FA deficiency is a known risk factor for neural tube defects, many professional organizations and governmental agencies recommend the use of daily supplements containing folic acid 2–3 months before conception and during pregnancy [3, 5].

We have observed in previous studies that a FAD maternal diet, at the gross ocular level, produces biometric changes in some eye structures [47], and at the tissue level [45, 46], alters expression of two extracellular matrix proteins, collagen IV and laminin-1, in lens and retina. In the present study, we expand on that work and use digital images from it to study changes in the cornea, lens, vitreous, and retina and to investigate the extent to which such changes generalize throughout the eye. To quantify alterations and distinguish between altered structures, we apply fractal and multifractal analysis at the tissue level [11, 52]. The methods and measures available for fractal and multifractal analysis, especially those applied to textures of biological images, are varied [10]; we use the fractal dimension (FD), lacunarity, multifractal spectrum, and Local Connected Fractal Dimension (LCFD) [54].

Due to the main objectives of the work we have improved the traditional fractal approach with an analysis of the multifractal spectrum and statistical resampling techniques:

a) Since the total number of individuals and sample size was relatively small, we have incorporated to the multifractal technique a statistical analysis using the bootstrap resampling techniques [6, 9, 15, 17] along with a non-parametric significance test: Kruskal-Wallis [44].
b) Each of these groups also presents a variability due to the individuals themselves. The objective of the present work isn´t only to distinguish between individuals within their own group, but to distinguish between individuals of the previous groups to determine if

Abbreviations: FAD, folic acid deficiency; FA, folic acid; FD, fractal dimension; Lac, lacunarity; Div, divergence.

* Corresponding author at: Department of Anatomy and Embryology, Faculty of Optics and Optometry, Universidad Complutense de Madrid, Calle de Arcos de Jalón, 118, Madrid 28037, Spain.
E-mail address: o.sijilmassi@ucm.es (O. Sijilmassi)

https://doi.org/10.1016/j.chaos.2020.109885
0960-0779/

the fractal structure of the tissues changes because of the maternal FAD diet or not. Due to this, it is also necessary to characterize the variance and covariance between the results of the individuals of the own group. For this purpose, statistical distance such as Mahalanobis distance [12] have been used. In this sense, metrics for the comparison between groups of multifractal spectrums are developed and explained in "materials and methods" section.

2. Materials and methods

2.1. Animals and diet

FA deprivation and immunohistochemistry experiments were performed as described previously [34, 45, 46]. All experiments were performed using protocols approved by the Animal Experimentation Committee of the Universidad Complutense of Madrid. As in the previous studies, we are going to analyse three sample groups: Control group: composed of embryos from females fed a standard diet of FA. D2 group: embryos from females fed a FAD diet during the first two weeks of pregnancy, finally, the D8 group, consisting of embryos from females fed a diet deficient in FA for 8 weeks: 6 before pregnancy and 2 during the two weeks of pregnancy. In turn, each of these groups contains two subgroups corresponding to labeling with anti-collagen IV or anti-laminin-1.

The number of pregnant mothers for each group (control, D2 and D8) was 9 and randomly an embryo was taken per mother. The number of embryos was $n = 9$ for each group. Thus, all embryos were studied on day 14.5 of gestation (E14.5). At this time of development, the basic structure of the eye is formed.

Although several embryos of the same mother could be analysed in our study, we decided to use them from different mothers so that the results were not biased by using only one mother.

Mouse embryos at 14.5 days of gestation (E14.5) were removed by cesarean section, placed in cold sterile phosphate-buffered saline (PBS) and decapitated. The heads were cut using a microtome set at 5 μm. Sections were placed on slides and collagen IV or laminin-1 staining was performed.

Immunohistochemistry in sections was visualized using a Leica DMRB microscope and photographed using Leica DFC 320 digital camera. The resolution of each image is 2088 × 1550 pixels in RGB. The pixel camera size is 3.45 μm x 3.45 μm with x10 magnification.

2.2. Multifractal analysis theory and application

As stated in the introduction section, the number of parameters that can be used, related to the multifractal analysis, is large and varied. In this section they are detailed those that have been used specifically in this article with a brief explanation of them.

2.2.1. Fractal dimension (D)

Fractal analysis is used to measure and characterize irregular or rough objects. A key feature of fractals is that they are non-trivially self-similar patterns that can be measured by a fractal dimension (FD) that may be a non-integer value [35]. Self-similar objects are characterized by being scale-free, i.e. at all scales it looks similar, despite a closer or a more distant look [29]. On the other hand, FD is a numerical measure that details the degree of irregularity of the contour or the roughness of the surface [14]. This measure is useful for describing how close a geometry is to being a point (0-dimensional sets), a straight line (1-dimensional sets), a plane (2-dimensional sets), or a volume (3-dimensional sets). To calculate this dimension there are several methodologies with their own theoretical bases [31]. The method used in the present work is the Box-Counting that was defined by Russell et al. [41]. This method consists in covering a given digital binary image with a set of measuring boxes of sizes ε. The number of squares L(ε) which encompass the object from the image is given by a power law and can be written in the following form:

$$L(\varepsilon) = \varepsilon^{-FD} \tag{1}$$

Then, as $\varepsilon \to 0$, the box-counting dimension (FD) can be estimated as:

$$FD = -\lim_{\varepsilon \to 0} \left(\frac{\log(L(\varepsilon))}{\log(\varepsilon)} \right) \tag{2}$$

It is important to consider that the boxes of size ε are non-empty sets to avoid the complications that may arise with log (0)and log (∞).

In the image processing programs, the program itself estimates, for a box size ε, the number of boxes $L(\varepsilon)$ needed to cover the entire image. Therefore, the FD is determined by plotting log $(L(\varepsilon))$ versus log (ε)where the size of the boxes is represented (x-axis) versus the number of boxes needed to cover the entire object (y-axis) [26]. Fig. 1 shows the number of boxes needed to completely cover images of the different structures of the eye studied: neural retina, vitreous, lens and cornea.

2.2.2. Lacunarity (Λ)

The FD is not a complete identifier of the texture of the tissue, so other concepts have been proposed to distinguish between structures that have the same FD but look different. One of these concepts is Lacunarity (Λ). It is a multiscale analytical measure that evaluates tissue heterogeneity. It has been defined as the degree of gappiness, heterogeneity, and translational and rotational invariance in an image [35, 40]. Generally, it used to determine the texture associated with patterns of spatial dispersion [13, 36]. The method for estimating lacunarity is the gliding box algorithm introduced by Allain and Cloitre [2]. To determine this variable in a completely correct way, the fluctuations of the mass distribution function of the pixels are analysed. The algorithm can be briefly described for a binary image as follows: an ε × ε box is placed at the upper left corner of an image. A value for the pixels of interest is chosen (e.g., black) for the entire image. Then, the number of black pixels in the box is counted. The box is moved one-pixel position and the number of pixels is counted again until the entire image is covered. The procedure is repeated over the entire image once for each ε.

If $n(M, \varepsilon)$ is the number of the gliding-boxes with mass M, the probability function $Q(M, \varepsilon)$ is obtained by dividing $n(M, \varepsilon)$ by the total number of boxes$L(\varepsilon)$of size ε

$$Q(M, \varepsilon) = \frac{n(M, \varepsilon)}{L(\varepsilon)} \tag{3}$$

The first and second moments of the distribution $Q(M, \varepsilon)$ are given by $\sum_M MQ(M, \varepsilon)$and $\sum_M M^2 Q(M, \varepsilon)$, respectively. Now, we can define lacunarity for this box size as:

$$\Lambda(\varepsilon) = \frac{\sum_M M^2 Q(M, \varepsilon)}{\left[\sum_M MQ(M, \varepsilon)\right]^2} = \frac{\sigma_\varepsilon^2}{\mu_\varepsilon^2} + 1 \tag{4}$$

where σ_ε^2 is the variance of the distribution $Q(M, \varepsilon)$ and μ_ε^2 is squared mean value of that distribution. Lacunarity depends on the scale ε. For large scales, the tissue tends to appear as homogeneous and the standard deviation is small. On the contrary, however, for small scales the standard deviation is greater, tissues will have a high lacunarity Δ(ε)pattern of texture due to greater variations in gap sizes. In general, lacunarity depends on the scaleεas $\Delta(\varepsilon) \sim \varepsilon^{-\beta}$, where the exponent β can be calculated by linear regression [43]. It must be borne in mind that lacunarity is a parameter that is sensitive to both image density and its spatial configuration [21].

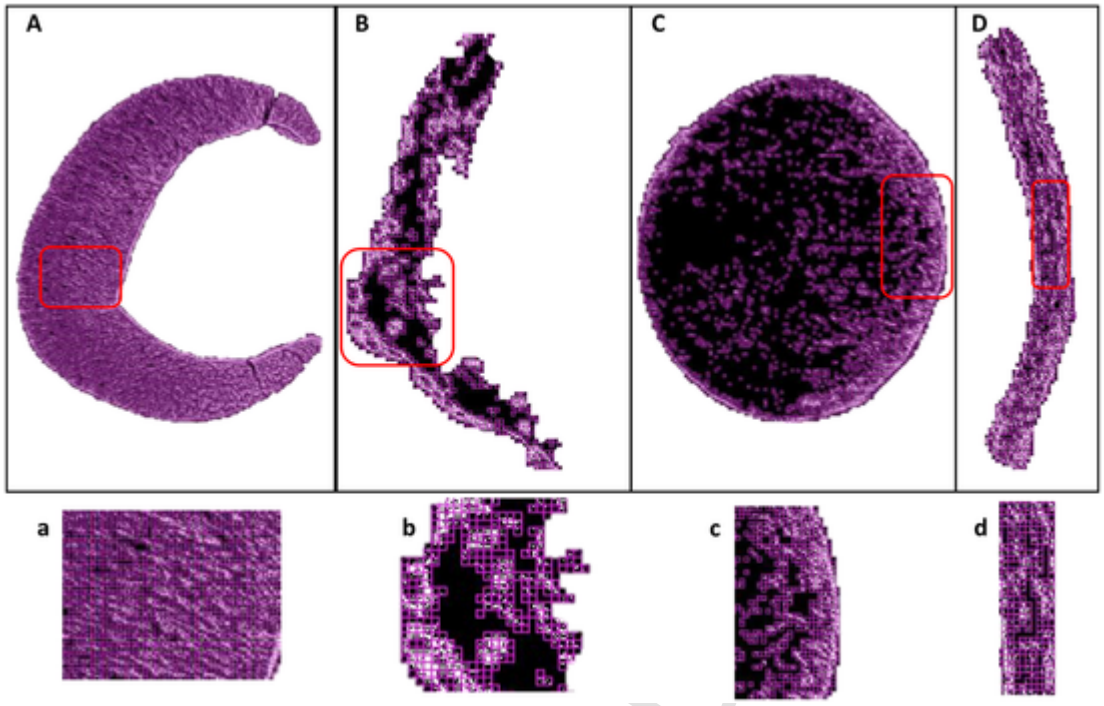

Fig. 1. Application of the box-counting method to different eye structures images from a normal mouse. To calculate fractal dimension, the whole image is covered with a set of squares with different lengths. For each grid the number of boxes covering the image are counted. Thus, the total number of boxes L(ε) covering the full image surface at the scale ε is computed with (Eq. (2)). From left to right, retina (A, a), vitreous (B, b), lens (C, c) and cornea (D, d)); a, b, c, and d images correspond to the magnified image regions (red rectangles) for A, B, C and D respectively. The boxes are clearly visible on a,b,c,d images.

2.2.3. Multifractal singularity spectrum

The singularity spectrum can be used to characterize a structure as mono- or multifractal [7, 43]. To measure it, the image is covered with various boxes size ε. Then, a probability can be defined for each box,$P_i(\varepsilon)$ as:

$$P_i(\varepsilon) = \frac{N_i(\varepsilon)}{N_T} \tag{5}$$

where $N_i(\varepsilon)$ is the number of pixels occupied (black pixels) in the box i, divided by the total number of pixels N_T. This measure gives us the probability that a pixel chosen at random belongs to the box i. In a homogeneous tissue the previous probability varies homogeneously with ε size as $P \sim \varepsilon^D$, where D is tissue´s fractal dimension FD. If the tissue is heterogeneous, the probability scales locally in different regions k of the tissue as $P(k,\varepsilon) \sim \varepsilon^{\alpha_k}$,$\alpha_k$ is the Lipschitz-Holder exponent or singularity strength [16]. If we measure now the number of boxes,$B(\alpha)$, whose singularities are in the interval $[\alpha, \alpha + d\alpha]$, we will see that they are scaled as $B(\alpha) \sim \varepsilon^{f(\alpha)}$; $f(\alpha)$is the FD of the set of boxes with singularitiesα [42]. For the calculation of $f(\alpha)$, it is usual to proceed as follows: from the Eq. (5), a probability measure $\mu_i(q, \varepsilon)$which dependents on a q parameter is defined as [7]:

$$\mu_i(q,\varepsilon) = \frac{\left(P_i(\varepsilon)\right)^q}{\sum_{j=1}^{L(\varepsilon)}\left(P_j(\varepsilon)\right)^q} \tag{6}$$

The parameter q acts as a magnifier. The values of $q > 1$ amplify the regions with high probability, while $q < 1$amplify the low probability ones. For a certain range of values of q [(−10,10), (−20, 20), etc.], the FD $f(\alpha(q))$ is calculated as the slope of the regression line of $\sum_i \mu_i(q,\varepsilon)\log\mu_i(q,\varepsilon)$ versus $\log(\varepsilon)$, while the singularity $\alpha(q)$ is calculated as the slope of the regression of $\sum_i \mu_i(q,\varepsilon)\log P_i(q,\varepsilon)$versus $\log(\varepsilon)$ [43]. Thus, for each value of q we have a pair $(\alpha(q), f(\alpha(q))$, known as the multifractal spectrum [19] with interesting properties: if the structure is monofractal its spectrum collapses to a single point. Contrariwise, if it is multifractal tends to have a wide spectrum whose maximum corresponds to the dominant singularityα_0.The value $f(\alpha_0)$would correspond to the fractal dimension D_0 that we would obtain by ignoring the multifractality and treating the tissue as monofractal [43]. The left part of the spectrum, measured from this α_0,corresponds to the large fluctuations ($q > 1$) while the right part corresponds to the small fluctuations ($q < 1$). Thus, in a multifractal structure the left part of the spectrum is often wider than the right part due to the structure heterogeneity (see Fig. 2).

The previous algorithm is implemented in FracLac [24]. In this work we have taken the curves (α, $f(\alpha)$) provided by the previous software along with a measure of the multifractality called *green divergence* or *divergence,* ρ. Divergence is based on the minimum and maximum values for the $f(\alpha)$versus α multifractal spectra for the two sets of values around each side of $q = 0$. Mathematically (Eq. (7)), it is the ratio of the areas defined by the spectra within those two spaces, × 100, calculated in the space defined by the Q_{set} used in determining the multifractal spectra ([25]b).

$$\rho = \frac{(\alpha_0 - \alpha_{\min})\cdot(f(\alpha_0) - f(\alpha_{\min}))}{(\alpha_{\max} - \alpha_0)\cdot(f(\alpha_0) - f(\alpha_{\max}))} \times 100 \tag{7}$$

To use it to compare patterns, the same Q_{set} for all images must be used. In our case this range goes from −30 to 30. For example, in the case of Fig. 2, ρ is equal to 100 because the multifractal part with large fluctuations is equal to the small fluctuations part. As can be seen in Fig. 2, the peak value of the multifractal spectrum corresponds to dominant singularity or D_0. The spectrum studies the degree of roughness, complexity, abnormality and asymmetry of tissues [7]. While, the curvature and symmetry of the $f(\alpha)$ spectra provide information on the heterogeneity [38]. From the curves of the multifractal spectrums, we can obtain the values of $\alpha_{\max}$ and $\alpha_{\min}$, which indicate the maximum and minimum fluctuation probability of the pixels, respectively [8]. From these parameters, we can calculate the width of singular-

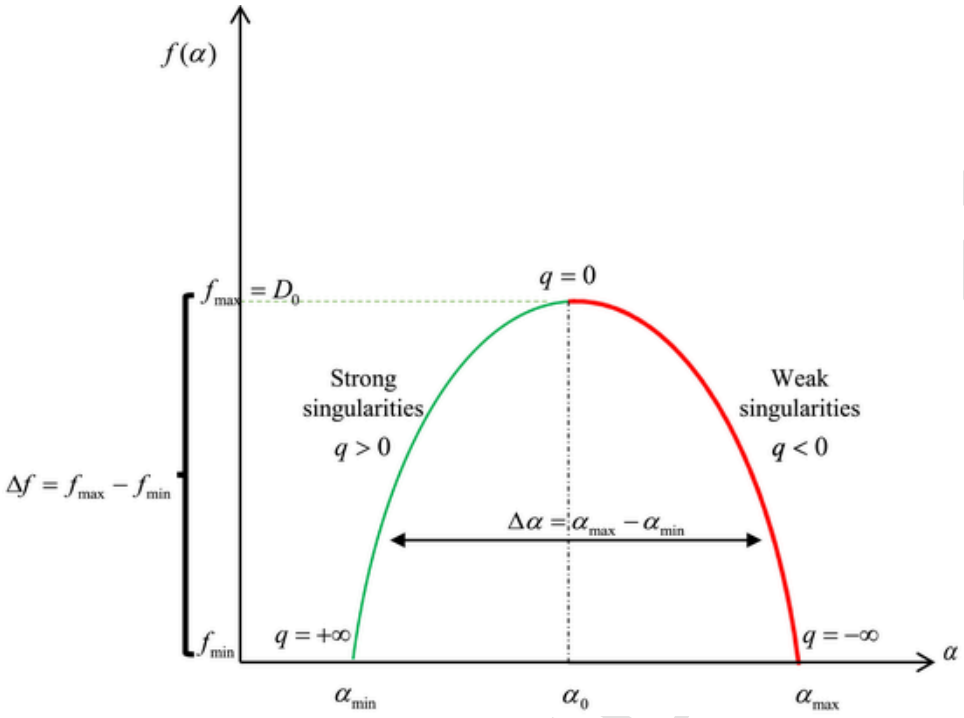

Fig. 2. Schematic presentation of main parameters of a multifractal spectrum: the maximum value of f (α) is D0, ($\alpha_{max}-\alpha_{min}$) measures the heterogeneity index which can be divided in two indices:, ($\alpha_{q+}-\alpha_0$) is for low values of α and ($\alpha_0-\alpha_{q-}$) is for high values, where α_{q-} and α_{q+} are the α values for the minimum and maximum value of q considered, respectively as ($\alpha_{q+}-\alpha_0$) and ($\alpha_0-\alpha_{q-}$) assess such quantity for high and low singularities, respectively.

ity strength $\Delta\alpha = \alpha_{max} - \alpha_{min}$, an index providing information about the heterogeneity of texture, i.e. it makes a quantitative determination of the degree of multifractality. Moreover, we have evaluated the asymmetry of the spectrum shape by the following formula [22, 49]:

$$A = \frac{\alpha_0 - \alpha_{min}}{\alpha_{max} - \alpha_0}, \tag{8}$$

where α_0 is the value of α when $f(\alpha)$ assumes its maximum value. The parameter A is also an important index of multifractality.

For each group of images (control, D2, and D8) we have a vector with the values of the fractal dimension, DF, divergence, Div, and Lacunarity, Lac, [DF, Div, Lac] that can be represented as a point in a 3D diagram. Each group will therefore have an average value of this vector given by $\left[\overline{D_F}, \overline{Div}, \overline{Lac}\right]$. In order to increase the accuracy of this average value, the following bootstrap procedure is performed.

a) From the values V (k) = [DF (k), Div (k), Lac (k)] k = 1,… .N images, the average value, $\bar{V}$, and the covariance matrix, S, were calculated for these variables within the same group of images.
b) The eigenvectors of the matrix S, $e_\alpha(k)$, allow to calculate new variables, given by $Y_\alpha(k) = \sum_{k=1}^{N} e_\alpha(k)\left(V(k) - \bar{V}\right)$, with α = 1,2,3, which are uncorrelated with each other.
c) The $Y_\alpha(k)$ sample is expanded by bootstrap to produce a better estimate of the average value of each of them $Y^{Boot}{}_\alpha(k)$.
d) Bootstrap estimates of the means are correlated again, undoing the previous base change, producing a bootstrap estimate of the means of the original variables such as $\left(V^{Boot}(k) - \bar{V}\right) = \sum_{\alpha=1}^{3} e_\alpha(k)\, Y_\alpha(k)$.
e) Finally, the Matlab Geom3d toolbox [27] is used to represent the dispersion of these points by means of an ellipsoid that can have an arbitrary orientation in the 3D-space ($\left[\overline{D_F}, \overline{Div}, \overline{Lac}\right]$), an option that Matlab's standard functions does not allow us. (The functions of Gem3d toolbox used are InertialEllipsoid, drawPoint3d, drawElliposid).”

2.3. Mathematical procedure to compare multifractal spectra

The previous section describes the procedure to obtain the multifractal spectrum of a given structure. In this work, we want to characterize the differences in the multifractal spectrum of ocular structures from three different sample groups: control group and two groups with maternal FAD diet (D2 and D8). Each of these groups has 18 eyes from different embryos; nine of them are labeled with anti-collagen IV and the other nine with anti-laminin-1. Four different structures (cornea, lens, retina and vitreous) of each eye were analysed. In total, 216 multifractal spectra are analysed. To extract information from them we have considered two comparison metrics. We have used several metrics to check the consistency of the results:

The first metric consists of the following: each multifractal spectrum obtained can be characterized by a vector $V_{g,i} = \left[\alpha_0, \Delta\alpha, f\left(\alpha_0\right), \Delta f, A\right]$, which describes the parameters, defined in the previous section, for the multifractal spectrum of the structures of the eye "i" belonging to the group "g" (control - C -, D2, and D8). The control group can be characterized by a mean vector $V_C = (1/N)\sum_{i=1}^{N} V_{C,i}$, where N is the number of eyes in the control group (C). A distance ($d_{g,i}$) between V_C and the spectrum represented by $V_{g,i}$ can be defined as:

$$d_{g,i} = \sqrt{\left(V_{g,i} - V_C\right)\cdot\left(V_{g,i} - V_C\right)^T} \tag{9}$$

The analysed structures of the control group will be at a mean distance from their mean vector V_C given by $\langle d_{C,i}\rangle_i$, where the subscript denotes that the average value should be taken by averaging over the studied structures of each eye. Finally, a distance between a certain group "g" and the control group C can be defined as:

$$d(g, C) = \frac{\langle d_{g,i}\rangle_i}{\langle d_{C,i}\rangle_i} \tag{10}$$

This distance measures the average difference of a group of structures of each eye with the average of the control, normalizing it by the average distance of the structures of the control group to its average. In this way, values greater than 1 show us how many times a certain structure of that eye differs from that of the control.

On the other hand, **the second metric** consists of the following: each multifractal spectrum is characterized by a vector $h_q = (\alpha(q), f(\alpha(q)))$, as described in the previous section. For each "q" the previous vector defines a two-dimensional statistical variable with a covariance matrix $\mathbf{S}_q$, considering a group of spectra (control, D2 and D8).

We can define the vector $h_q^C = (1/N)\sum_{i=1}^{N}\left(\alpha_i(q), f_i(\alpha(q))\right)$as the mean vector which characterizes the control group, being N the number of eyes in the control group. At each point "q", the control group will have a covariance matrix $\mathbf{S}_q^C$.

For each spectrum of each eye "i" within a certain group "g" and for each point "q" of the spectrum, we can define a distance such as:

$$\Omega_q^{g,i} = \sqrt{\left(h_q^{g,i} - h_q^C\right)^T \cdot \left[\mathbf{S}_q^C\right]^{-1} \cdot \left(h_q^{g,i} - h_q^C\right)} \tag{11}$$

This distance is Mahalanobis' Distance [12, 33] between a point of the spectrum and the average of the control group, for a given "q". It measures the distance between these two points but normalizes it by the standard deviation of the data in the direction of the point $h_q^{g,i}$considered. From the definition of Eq. (11) we can give the distance of a spectrum considered respect to the control spectrum as a mean value given by $\Omega^{g,i} = \left\langle \Omega_q^{g,i} \right\rangle_q$, where the subscript "q" means that the average should be taken in "q". Finally, we can define the distance of a group "g" to the control, $\Omega(g, C)$ as:

$$\Omega(g, C) = \left\langle \Omega^{g,i} \right\rangle_i \tag{12}$$

Analogously, we can also study the value of these distances for each point "q" by means of:

$$\Omega_g(q) = \left\langle \Omega_q^{g,i} \right\rangle_i \tag{13}$$

This last distance $\Omega_g(q)$ gives us information about which part of the spectrum ($q < 1$ or $q > 1$) has greater variations with respect to the control group. This provides us one more parameter to analyse if the difference between the structures occurs much more in the monofractal or multifractal part.

2.4. Tests of statistical significance

As we mentioned above, we have also calculated the FD, lacunarity "Lac" (mean value of $\sigma_\varepsilon^2/\mu_\varepsilon^2$ defined in Eq. (4), over the box size ε and grid orientations) [24], and divergence (Div) mean values, for all groups and samples. For small sample sizes, as in our case, the bootstrap method for estimating their distributions is given. Bootstrapping is a resampling technique used to estimate statistics from the original sample by sampling with replacement [15]. We can use it to estimate summary statistics such as the mean, standard deviation, skewness and kurtosis. For an overview, interested readers are referred to [6]. In this work a total of 100 bootstrap replicas have been used. This number of replicas should be enough to give us the confidence levels we need [17]. Moreover, it seems to be appropriate for most of the applications in which the authors have worked. Afterward, a rank-based nonparametric test termed the *Kruskal–Wallis test* is used to determine if there are statistically significant differences between the control and the other groups. The idea of the Kruskal–Wallis rank test is to compare medians among k comparison groups (in our case $k = 3$). The hypothesis tested must determine whether the medians of two groups (control and D2 or control and D8) are different. The null and alternative hypotheses for the Kruskal Wallis nonparametric test are stated as follows for each structure studied:

- Null Hypothesis: all group medians are equal.
- Alternative Hypothesis: not all group medians are equal.

2.5. Digital image processing

For multifractal fractal analysis images were opened in the image analysis program ImageJ [39]. Then, in each original colour image it was selected four regions of interest (ROI): cornea, lens, retina and vitreous. A total of 54 eyes were analysed. Thus, in order to all images have similar degree of detail sharpening was applied. On the other hand, for the multifractal spectrum calculations to have the same degree of stability and precision, a similar level of detail and contrast is required for all images, which is achieved by enhancing the contrast by a minimum of 30%. Since this process can also enhance noise and artefacts, for this reason the Despeckle was also performed. Therefore, each ROI was pre-processed by applying the following protocol/pathway: (ImageJ > Process > Sharpening), (ImageJ > Process > Enhance Contrast (30%)), (ImageJ > Process > Noise > Despeckle), and (ImageJ > Process > Binary > Make Binary). There are several methods for calculating fractal and multifractal measures [18]. In our study, multifractal analysis was performed using FracLac a plugin of ImageJ software of the National Institutes of Health [24]. Multifractal analysis was applied to all ROI's by using the following setting: ImageJ > Plugins > Fractal analysis > FracLac. Once the image is binarised, only the structure to be analysed is selected by means of ImageJ tools.

As an example, Fig. 3 shows the pre-fractal processing procedure applied to a mouse embryonic lens stained with anti-collagen IV.

The statistical processing of the results obtained with ImageJ was done using Matlab (The MathWorks Inc [51]).

3. Results

The results for multifractal spectrum and lacunarity, depending of the analysed eye structure (cornea, lens, retina and vitreous) are given in Figs. 4, 5, 6 and 7, respectively.

Lacunarity values depends on the box-size and on the distribution of the gaps: low lacunarity implies homogeneity, as all gap sizes are the same, whereas a higher lacunarity implies more heterogeneity which means the texture has variable holes. In all cases, figures show that as the box size increases, the lacunarity value decreases. In the other hand, in most cases, D2 and D8 are more lacunar (tissues have larger gaps) than the control except for corneas and retinae stained with anti-laminin-1.

The $-\beta$ exponent gives us information about how the homogeneity of the tissue changes with scale observation. A null value of β tells us that the tissue appears uniform regardless of the scale. In this way, we have seen that in both the lens and vitreous this heterogeneity with the scale tends to increase. On the contrary, in the case of the retina and cornea, it tends to decrease in both types of labeling: anti-collagen IV or anti-laminin-1. Even though it seems that for the case of corneas marked with anti-laminin-1, this value is almost the same as in the Control.

It is also seen from figures (4D, 5B, 5D, 7B and 7D) that D8 group exhibits the most heterogeneous tissues amongst all samples, indicating a more complex spatial arrangement. Figs.s (4 (A,C), 5 (A,C), 6 (A,C), and 7 (A,C)) show the multifractal spectra corresponding to the different tissues stained with anti-collagen IV or anti-laminin-1.

In the previous section we have defined certain parameters to compare the multifractal spectrums between control group and D2 and D8 groups. The results are given in Tables 1 and 2.

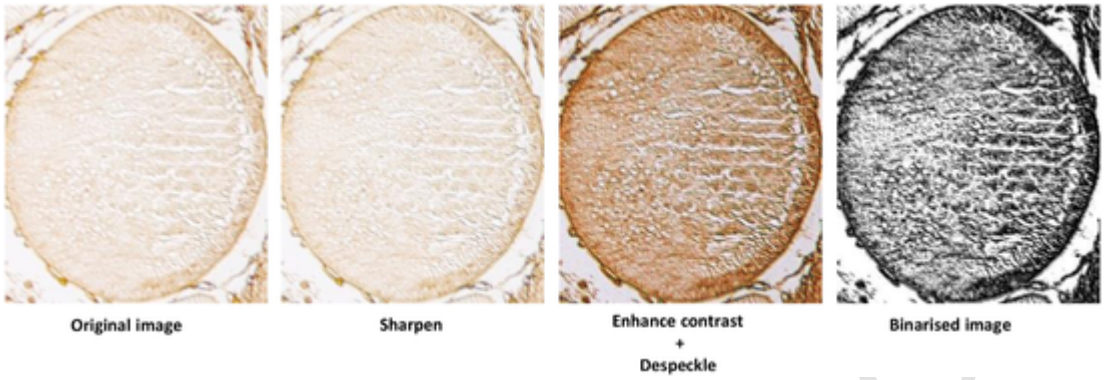

Fig. 3. From left to right, an embryonic lens labeled with anti-collagen IV, and the processing after sharpening, enhance contrast, noise reduction and binarization. All the pre-processing is done with ImageJ functions.

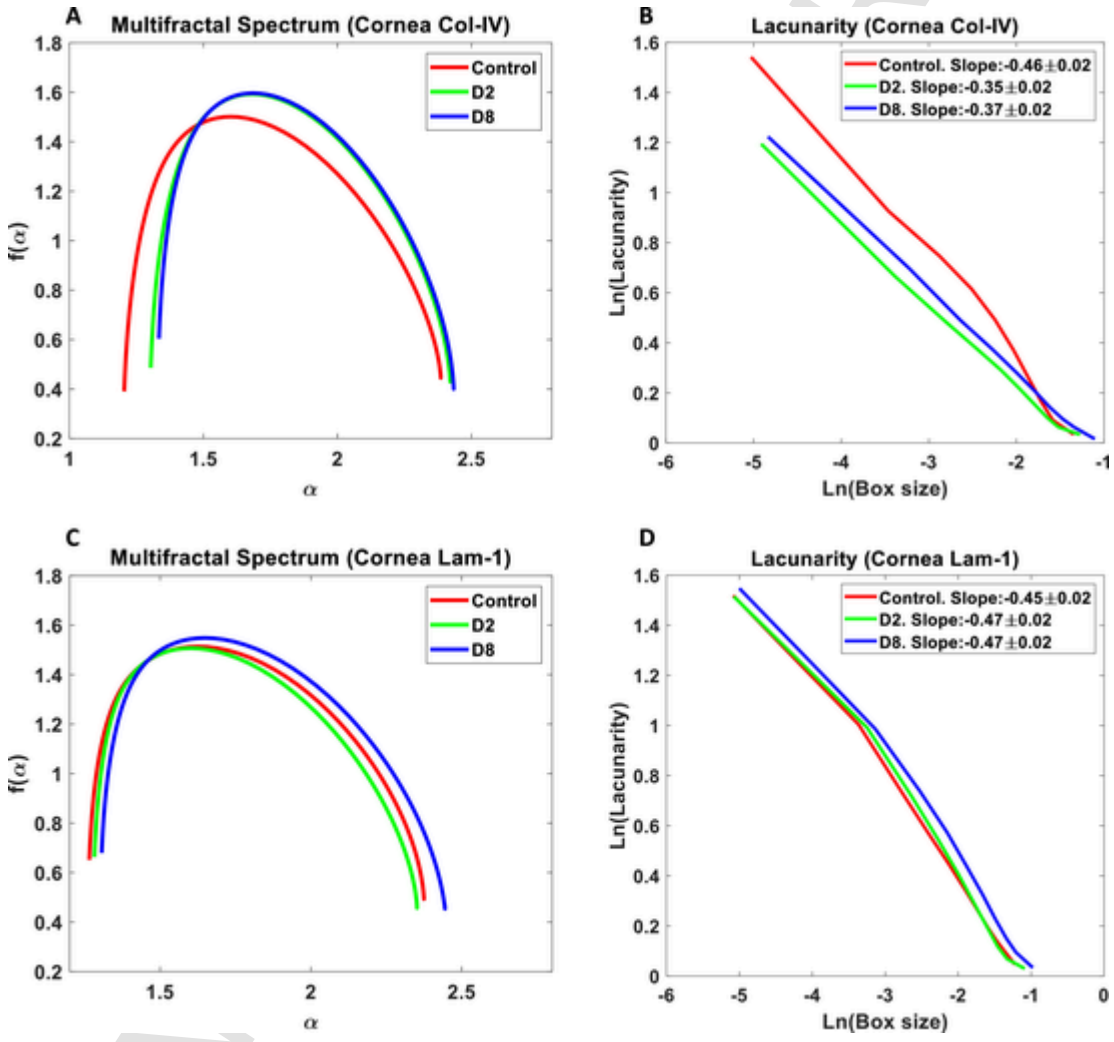

Fig. 4. Multifractal spectrums and lacunarity curves of corneas stained with anti-collagen IV (A and B) or anti-laminin-1 (C and D), for all groups.

For D2 and D8, values of the parameter $\Delta\alpha$ shown that lenses, retinae and vitreous stained with anti-laminin-1 as well as vitreous stained with anti-collagen IV have a larger values of $\Delta\alpha$than the control, which indicates the presence of a strong degree of multifractality in these structures. However, the cornea of both groups exhibited lower multifractality degree than the control, for both collagen IV and laminin-1.

On the other hand, the asymmetry presents three shapes: asymmetry to the right-skewed ($A > 1$), left-skewed ($A < 1$) or symmetric ($A = 1$). All samples for the three groups were observed to have values of $A < 1$, hence the curve of multifractal spectrum was left-skewed. A left-skewed spectrum denotes high fractal exponents and large fluctuations in the data. Tables 1 and 2 also reveal that, for deficient groups, corneas, lenses and vitreous stained with anti-collagen IV as well as lenses and vitreous stained with anti-laminin-1 have higher values of A than the control. In summary, in the most cases of our multifrac-

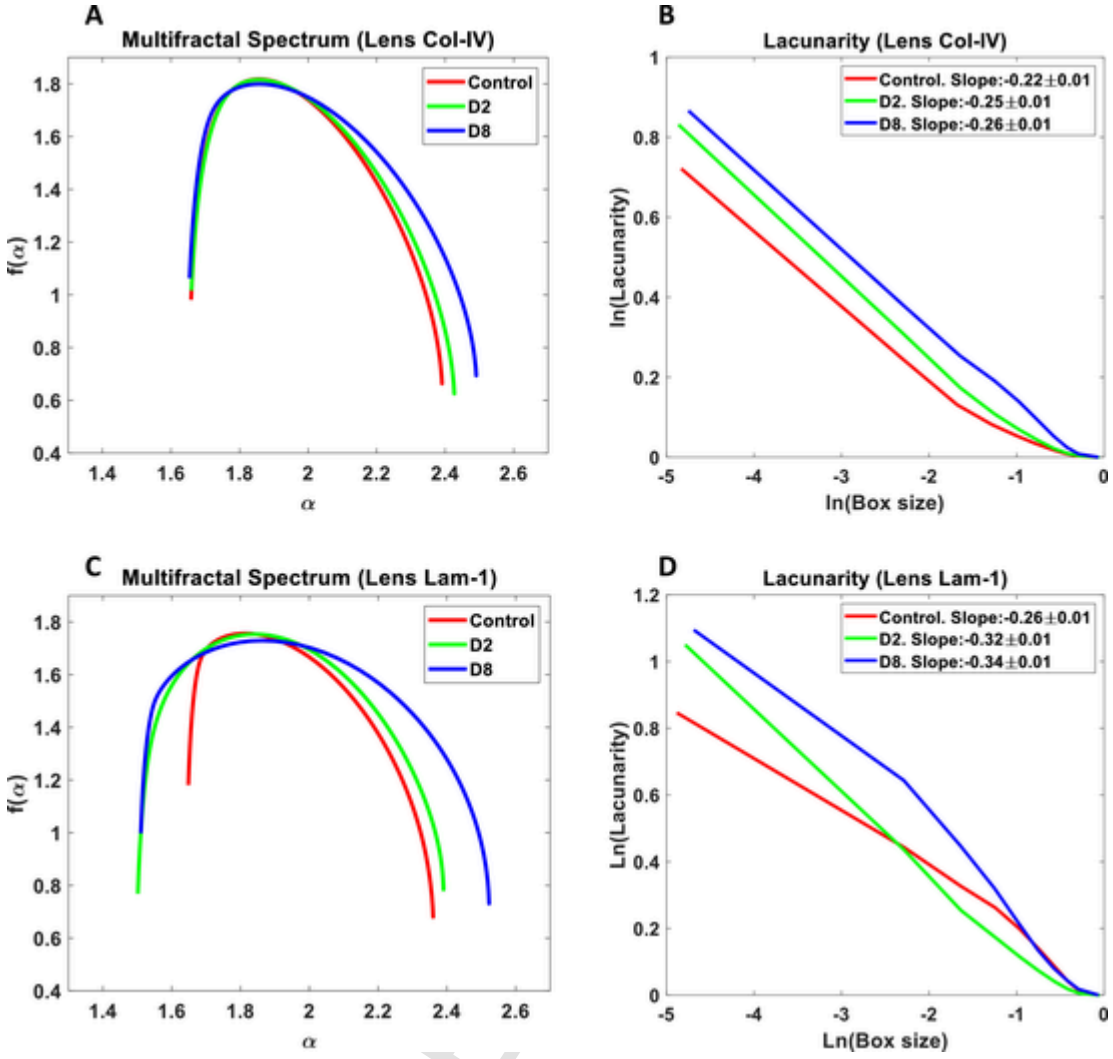

Fig. 5. Multifractal spectrums and lacunarity curves of lenses stained with anti-collagen IV (A and B) or anti-laminin-1 (C and D), for all groups.

tal spectra, the spectrum showed distinctively different shape and symmetry between control and D2 or D8 groups.

Regarding the results of $d(g, C)$(see Tables 1 and 2), considering that this metric is normalized by the scale of the control group (see Eq. (10)), values higher than 1 show relevant changes with respect to the control group. The results show that the distance with respect to the control is high in the case of the labeling with anti-laminin-1, especially in the lens and vitreous. In addition, the variability of this distance is very large in those cases (see standard deviation in the Tables 1 and 2). On the other hand, the structures marked with anti-collagen IV show a distance only slightly higher (see case of retina and cornea) than the control group. Finally, the distance with respect to the control is not significant in some structures marked with anti-laminin-1 (cornea, retina, and vitreous) and anti-collagen IV (lens and vitreous).

Regarding the second metric $\Omega(g, C)$, the distance with respect to the control group increases significantly in the structures labeled with anti-laminin-1 (vitreous, lens, and retina) and with anti-collagen IV (cornea, lens and retina). On the other hand, the distance is slightly greater in the corneas marked with anti-laminin-1 and remains practically the same in the case of the vitreous marked with anti-collagen IV. The greatest difference with the control group occurs in the case of the lens and the retina, both marked with anti-laminin-1 or with anti-collagen IV.

This second metric also allows us to make a comparison for each value of the parameter "q" in the multifractal spectra (see Eq. (13)). In Fig. 8 it is possible to see, the parameter $\Omega_g(q) = \left\langle \Omega_q^{g,i} \right\rangle_i$ averaged for eyes of the same group, some structures with the greatest distances respect to control (Fig. 8 up) and others with minimal important differences (Fig. 8 down). This figure allows us to compare in which part of the multifractal spectrum the greatest difference occurs ($q < 0$ monofractal part, $q > 0$ multifractal part). As can be seen, in the case of larger values (Fig. 8 up), the difference with the control group is in the multifractal part of the spectra mainly. In the case of the less important differences (Fig. 8 down), the changes affect the monofractal and multifractal part equally.

Results of statistical analysis are summarized in Tables 3 and 4. Both tables report the descriptive statistics of the variables (FD, Lac, Div) for the different eye structures studied. After applying the significance test described in the previous section, if the p-value is less than 0.05, there are significant differences between the groups. In this case, we reject the null hypothesis and accept the alternative hypothesis. On the other hand, if p-value is greater than 0.05 an asterisk marks the parameters whose difference with respect to the control are not statistically significant. As can be seen, in almost all cases, all parameters of the probability distributions have significant differences. Which

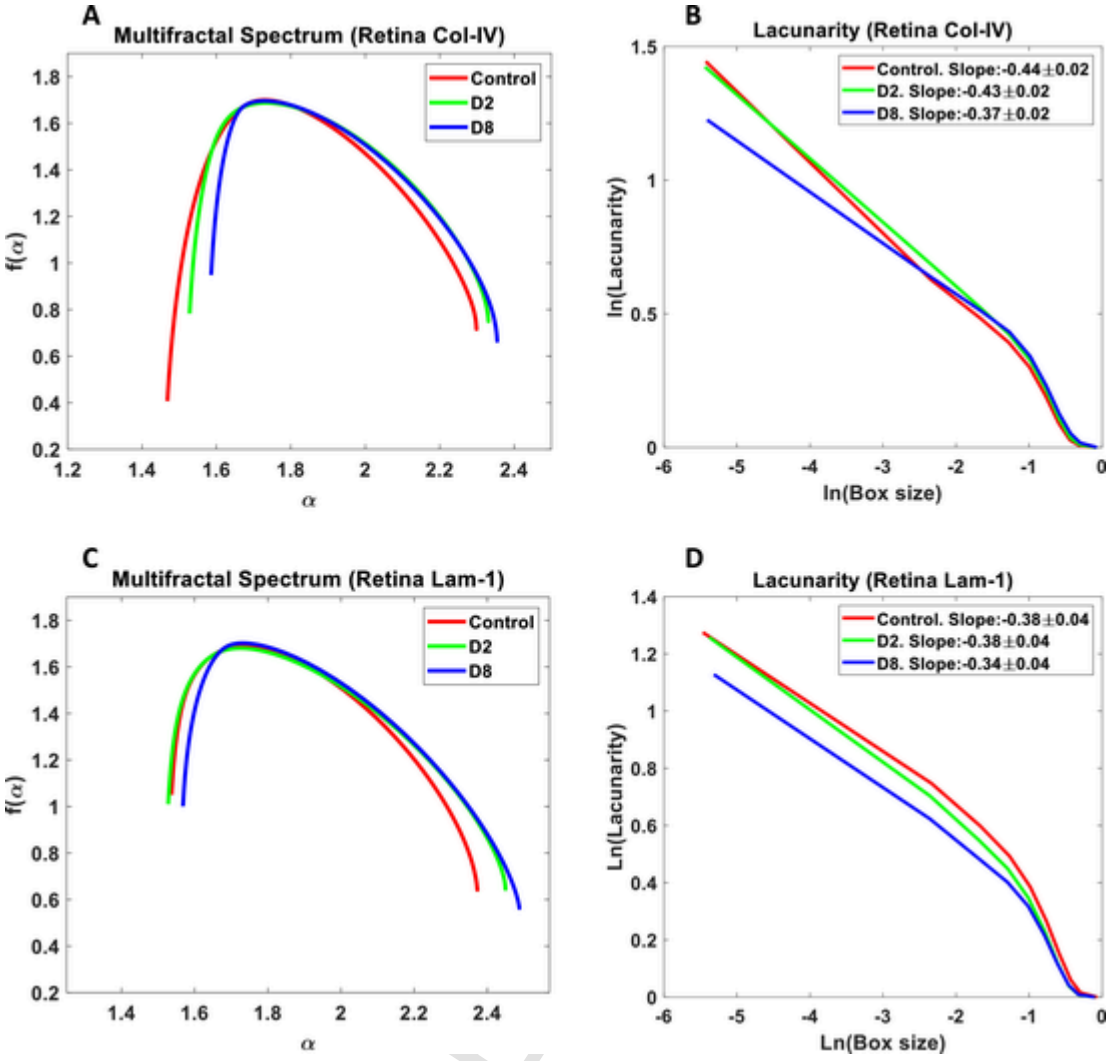

Fig. 6. Multifractal spectrums and lacunarity curves of retinae stained with anti-collagen IV (A and B) or anti-laminin-1 (C and D), for all groups.

shows that changes in the fractal structure of the tissue are already produced from a very short-term of maternal FAD diet (D2 group). To make these tables easier to understand, we use an ellipsoid function of Matlab to fit the measurements (FD, Lac, and Div) to an ellipsoid surface. Figs. 9 and 10 show the value of the bootstrap estimate the FD, lacunarity and divergence mean values along with their uncertainty intervals using the shape of ellipsoids in space [27], for the different structures studied. The differences with the control group are evident in practically all structures. The different orientation of the ellipsoids also informs us that the correlation between these three variables (FD, Lac, Div) changes between the control, and D2/D8 groups.

As show in Figs. 9 and 10, corneas stained with anti-collagen IV or with anti-laminin-1, for D2 and D8, have highest FD and lacunarity values than the control whereas both groups have lower divergence value. On the other hand, for D2 and D8, lenses stained with anti-collagen IV have smaller FD and divergence values than the control as well as highest lacunarity. Respect to retinae stained with anti-collagen IV or with anti-laminin-1, D2 and D8 have the lowest values of FD and divergence whereas the control experiencing the highest values. Retinas marked with anti-collagen IV have highest lacunarity value for D2 and D8 than the control, whereas retinas stained with anti-laminin-1 have lowest lacunarity value for D2 and D8 than the control. Finally, vitreous labeled with anti-collagen IV or anti-laminin-1 exhibit higher values of FD and divergence than the control; however, both cases present lower value of lacunarity with respect to healthy controls.

4. Discussion

This research describes the application of multifractal analysis to detect textural irregularities in embryonic eye structures due to maternal FAD diet. In the present paper, we use lacunarity for its ability to distinguish spatial patterns as well as to measure tissue heterogeneity [48]. The results show that it tends to increase in deficient groups with respect to the control. These findings show that highly lacunar tissues (D2 and D8) possess large gaps or low-density holes, while control group appear homogeneous. In a previous study [45], we have shown evidences that maternal FAD diet alters both ECM proteins, collagen IV and laminin-1, during eye development producing changes in their roughness and smoothness degree.

On the other hand, we have used two comparison metrics, $d(g, C)$and $\Omega(g, C)$. The first one informs us about changes in the fractal spectrum form, and the second tells us if the change occurs in the monofractal or multifractal part. Our results indicate that laminin-1 is more altered than collagen IV. Likewise, in some cases, changes occur both in the multifractal ($q > 0$)and monofractal($q < 0$)parts, depending on tissue studied as well as on the type of labeling. It is known [28, 32] that changes in the spatial distribution of ECM proteins have serious consequences for cell behavior. The authors consider that

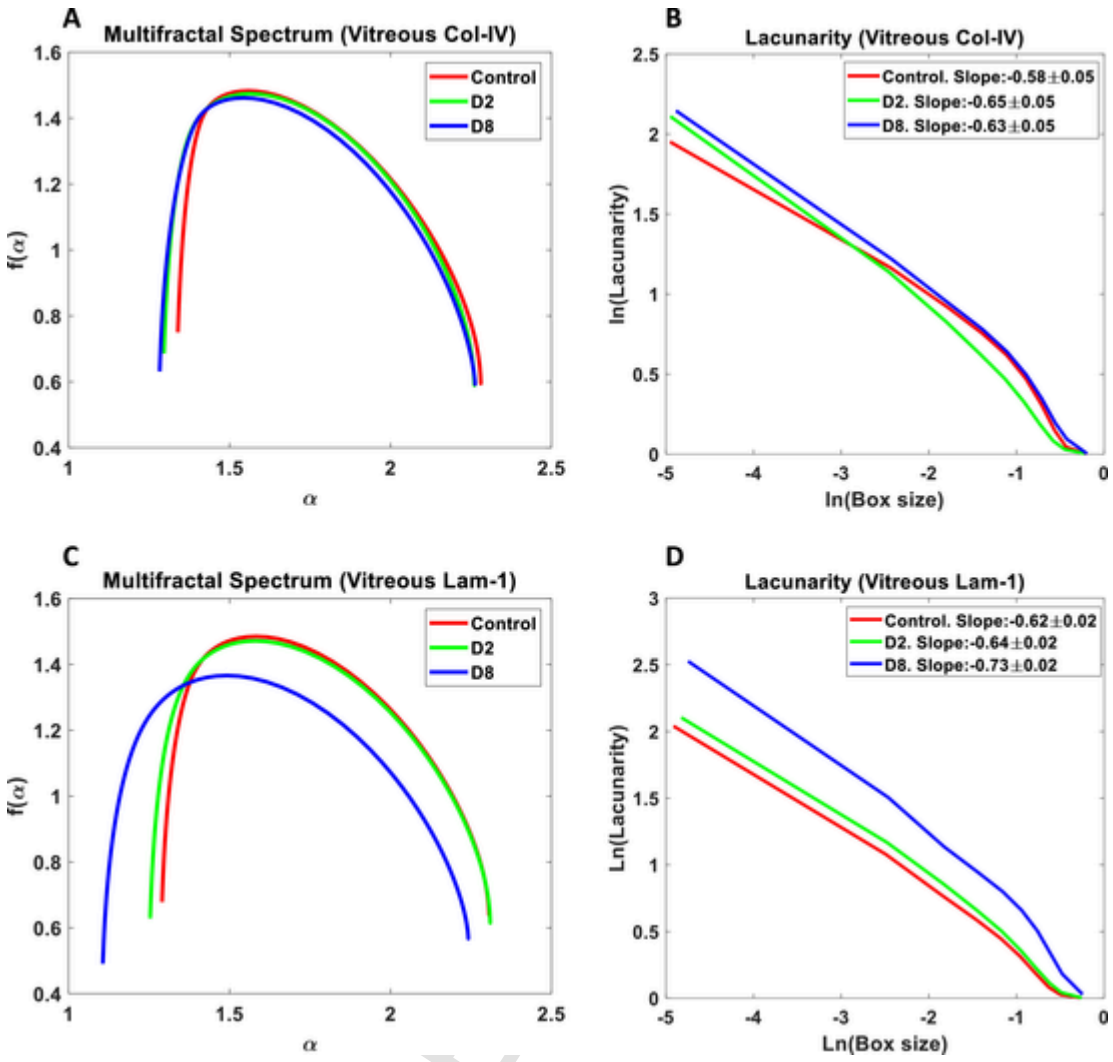

Fig. 7. Multifractal spectrums and lacunarity curves of vitreous stained with anti-collagen IV (A and B) or anti-laminin-1 (C and D), for all groups.

Table 1
Parameters obtained from multifractal spectrum of the cornea and lens for all analysed cases. C: control group. D2 and D8: deficient groups.

Structure	Cornea						Lens					
Stain	Col-IV			Lam-1			Col-IV			Lam-1		
Group	C	D2	D8	C	D2	D8	C	D2	D8	C	D2	D8
α_0	1.59	1.68	1.70	1.62	1.64	1.69	1.83	1.82	1.91	1.86	1.93	1.92
$\Delta\alpha$	1.22	1.01	1.22	1.14	1.06	1.26	0.62	0.63	0.98	0.83	0.91	1.02
$f(\alpha_0)$	1.52	1.62	1.61	1.44	1.56	1.60	1.83	1.76	1.78	1.82	1.85	1.80
Δf	1.37	1.28	1.31	0.88	1.11	1.28	1.38	1.02	0.98	1.22	1.53	1.16
A	0.33	0.41	0.45	0.83	0.35	0.47	0.22	0.28	0.59	0.31	0.41	0.40
$d(g, C)$		1.3 ± 0.4	1.5 ± 0.5		1.2 ± 0.4	1.0 ± 0.4		1.0 ± 0.6	1.1 ± 0.4		2.2 ± 1.1	2.2 ± 1.4
$\Omega(g, C)$	1.2 ± 0.5	1.7 ± 0.4	1.8 ± 0.3	1.2 ± 0.3	1.6 ± 0.4	1.4 ± 0.5	1.2 ± 0.3	1.5 ± 0.6	1.9 ± 0.6	1.3 ± 0.2	3.1 ± 1.2	2.7 ± 1.3

changes in both metrics imply altered organization of collagen IV and laminin-1 into tissues which could induce tissue damage. The authors have also shown changes in the spatial expression patterns of both molecules (i.e. an overexpression of collagen IV or laminin-1 due to maternal FAD) [46]. It is possible that overexpression of these proteins is implicated in the multifractal spectrum differences observed between the control and deficient groups.

The present study confirms the findings about changes in the organization of laminin-1 and collagen IV within the different eye structures. All of those techniques used in our study can be applicable to biological and medical image analysis. We strongly recommend using these tools fundamentally to determine if a given protein has an altered spatial organization. It is of great scientific and clinical interest to have determined that these parameters can be evaluated as markers of anomalies and might be applicable to other tissues. In our knowl-

Table 2
Parameters obtained from multifractal spectrum of the retina and vitreous for all analysed cases. D2 and D8: deficient groups.

Structure	Retina						Vitreous					
Stain	Col-IV			Lam-1			Col-IV			Lam-1		
Group	C	D2	D8	C	D2	D8	C	D2	D8	C	D2	D8
α_0	1.65	1.73	1.73	1.71	1.69	1.72	1.57	1.56	1.38	1.51	1.61	1.34
$\Delta\alpha$	0.72	0.73	0.86	0.81	0.99	0.78	0.67	0.78	1.33	0.92	1.06	1.38
$f(\alpha_0)$	1.63	1.71	1.72	1.69	1.69	1.72	1.58	1.51	1.25	1.44	1.50	1.17
Δf	1.14	0.92	1.26	1.09	1.23	1.32	0.77	1.0	1.25	0.84	1.03	1.20
A	0.21	0.22	0.21	0.20	0.05	0.16	0.09	0.30	0.61	0.22	0.47	0.72
$d(g, C)$		1.5 ± 0.4	1.5 ± 0.3		1.0 ± 0.5	1.0 ± 0.3		0.8 ± 0.6	1.2 ± 0.9		1.1 ± 0.6	1.8 ± 1.1
$\Omega(g, C)$	1.2 ± 0.4	1.7 ± 0.6	1.8 ± 0.2	1.2 ± 0.4	1.7 ± 0.7	2.1 ± 0.5	1.2 ± 0.4	0.9 ± 0.5	1.5 ± 0.9	1.2 ± 0.3	1.4 ± 0.7	3 ± 2

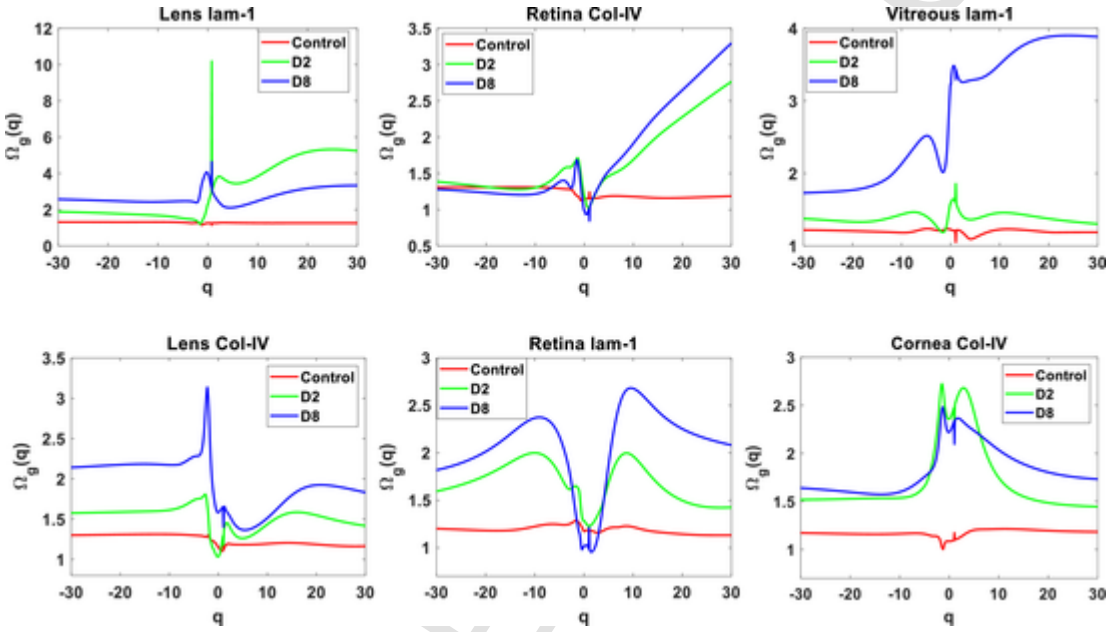

Fig. 8. Values of the metric defined by Eq. (13), for the most relevant cases (upper row) and for the distances slightly higher than the control group (lower row). In the case of greater distances, the greatest difference between the spectra of the different groups occurs in the multifractal part $q > 0$.

edge, no studies so far have linked multifractal changes in tissues to molecular expression patterns. The results presented in the present research have demonstrated that this method would be advantageous objective tool for tissue characterization and diagnosis, specially to quantify damage in the texture of biological tissues.

5. Conclusions

Biological tissue can be considered to be organized self-similarly at different scales but can also vary within itself, as measurable by fractal and multifractal features. In the present work, we analysed ocular tissue texture in embryos from mothers subjected to a FAD diet for two and eight weeks respectively. We applied several fractal metrics to cornea, lens, retina, and vitreous, finding the multifractal spectrum and lacunarity most promising to distinguish tissue changes associated with maternal FAD diets. Indeed, the results indicated that only two-weeks of a maternal FAD diet induced significant increases in tissue multifractality and heterogeneity.

CRediT author statement

Ouafa Sijilmassi: Investigation, Software, Formal analysis, Visualization, Writing - Original Draft, Writing - Review & Editing.

José Manuel López-Alonso: Conceptualization, Software, Formal analysis, Writing - Review & Editing, Supervision.

Aurora del Río Sevilla: Resources, Supervision, Writing - Review & Editing,

María del Carmen Barrio Asensio: Resources, Supervision, Writing - Review & Editing

Uncited reference

.

Declaration of Competing Interest

None.

Funding

This study was supported by grants to the Complutense Research Group 920202 from the Spanish Ministerio de Sanidad (PI06/0184 and PS09/01762). Likewise, it was supported by grants from the Spanish Ministerio de Economía y Competitividad (TEC2013-40442). Finally, this article was done with a pre-doctoral fellowship awarded by Complutense University of Madrid and Banco Santander (reference number CT27/16-CT28/16).

Table 3
Statistical Values for mean μ, standard deviation σ, skewness and Kurtosis of all samples for D2 group compared with the control.

Structure	Stain	Parameters $\begin{bmatrix} \mu & \sigma \\ Skewness & Kurtosis \end{bmatrix}$		
		FD	Lac	Div
Cornea	Collagen IV	1.55, 0.06 0.03, 1.62	0.23*, 0.04* 0.30*, 1.86	50.96, 19.32 0.35*, 1.78
	Laminin-1	1.49, 0.06 0.15, 2.40	0.29, 0.09 0.77*, 1.85	36.55, 20.71* 0.15, 1.56
Lens	Collagen IV	1.78, 0.02 −0.03, 1.69	0.33, 0.10 0.83*, 2.58	23.08, 15.95 1.11, 2.68
	Laminin-1	1.77, 0.07* −0.34, 1.89	0.37, 0.07 0.43*, 1.97*	79.79, 57.86 0.70, 2.25*
Retina	Collagen IV	1.64, 0.02 −0.12, 2.13	0.363, 0.04 1.08, 2.55	34.11, 14.87 0.36, 2.28
	Laminin-1	1.63, 0.02 0.15*, 1.85*	0.39, 0.06 1.06, 2.54	20.63*, 13.55 0.64, 2.18*
Vitreous	Collagen IV	1.48*, 0.04 −0.51, 1.74*	0.52, 0.06 −0.28, 2.12*	35.61, 18.62 1.01*, 2.48*
	Laminin-1	1.47, 0.06 −0.56, 2.31*	0.54, 0.14 0.21*, 1.67*	46.25, 24.11* 0.71, 2.19*

Table 4
Statistical Values for mean μ, standard deviation σ, skewness and Kurtosis of all samples for D8 group compared with the control.

Structure	Stain	Parameters $\begin{bmatrix} \mu & \sigma \\ Skewness & Kurtosis \end{bmatrix}$		
		FD	Lac	Div
Cornea	Collagen IV	1.59, 0.06 −0.49*, 2.18*	0.25, 0.03 0.09, 2.30	40.18, 21.61 0.75, 2.05
	Laminin-1	1.49, 0.06 −0.64, 2.56	0.30, 0.06* 0.32, 2.35*	34.88, 11.28 0.32, 2.11
Lens	Collagen IV	1.76, 0.03 0.29, 1.57	0.41, 0.17 0.38, 1.58	23.31, 12.7 0.29, 2.01
	Laminin-1	1.68, 0.09 −0.13, 1.52	0.50, 0.11* 1.23, 2.64	54.27, 56.89 0.90, 2.61
Retina	Collagen IV	1.66, 0.02 0.20, 2.12	0.38, 0.04 0.41*, 2.00*	17.94, 7.88 0.67, 2.28
	Laminin-1	1.65,0.02 −0.23, 1.70*	0.37, 0.03 1.00, 2.67	13.52, 7.44 0.63, 2.55*
Vitreous	Collagen IV	1.44, 0.11 −1.06, 2.46	0.53, 0.12 −0.23, 1.73	38.10, 27.85 0.77, 2.10
	Laminin-1	1.36, 0.12 −0.48, 1.81	0.53,0.21 0.89, 2.15	61.21, 42.60 0.55, 1.87

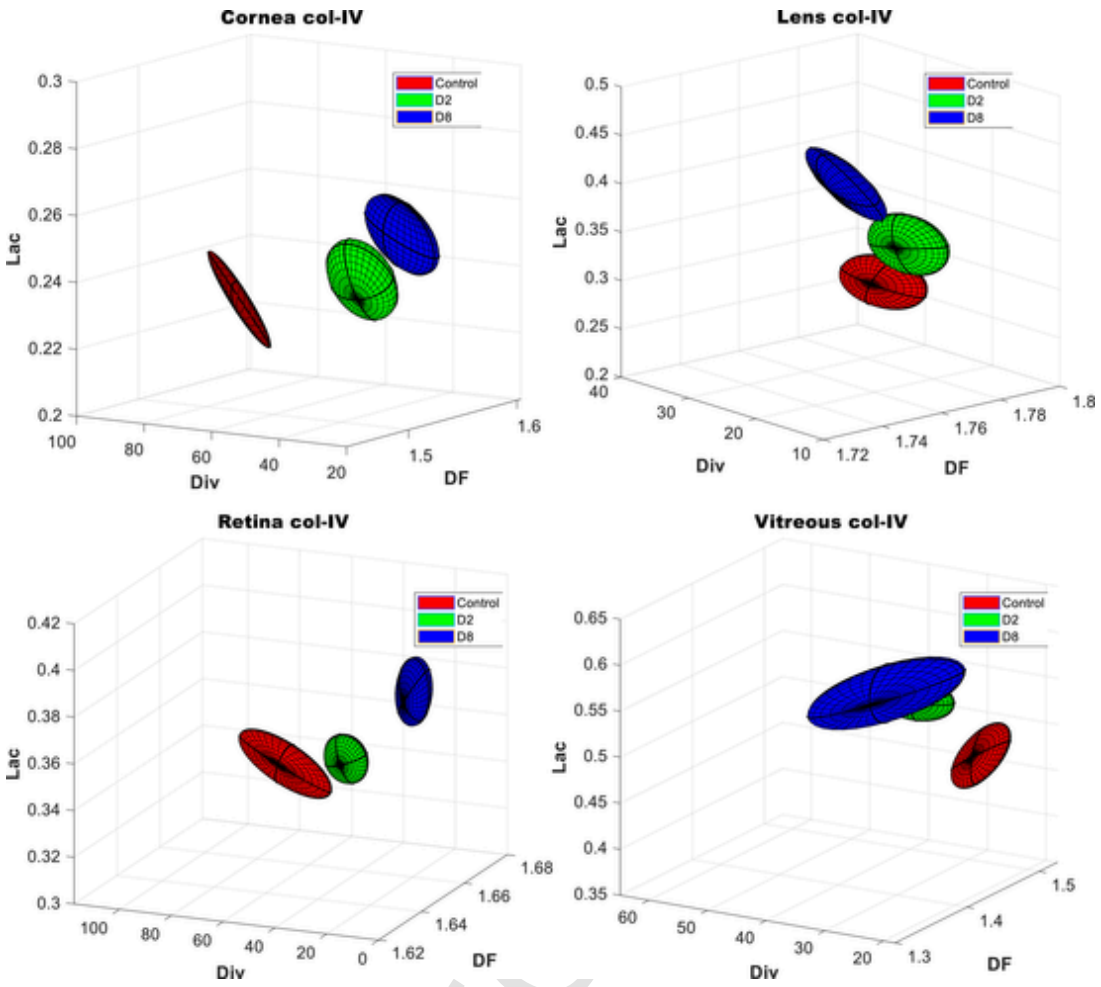

Fig. 9. graphical representation as ellipsoids for the mean´s distribution data, for all the structures stained with anti-collagen IV.

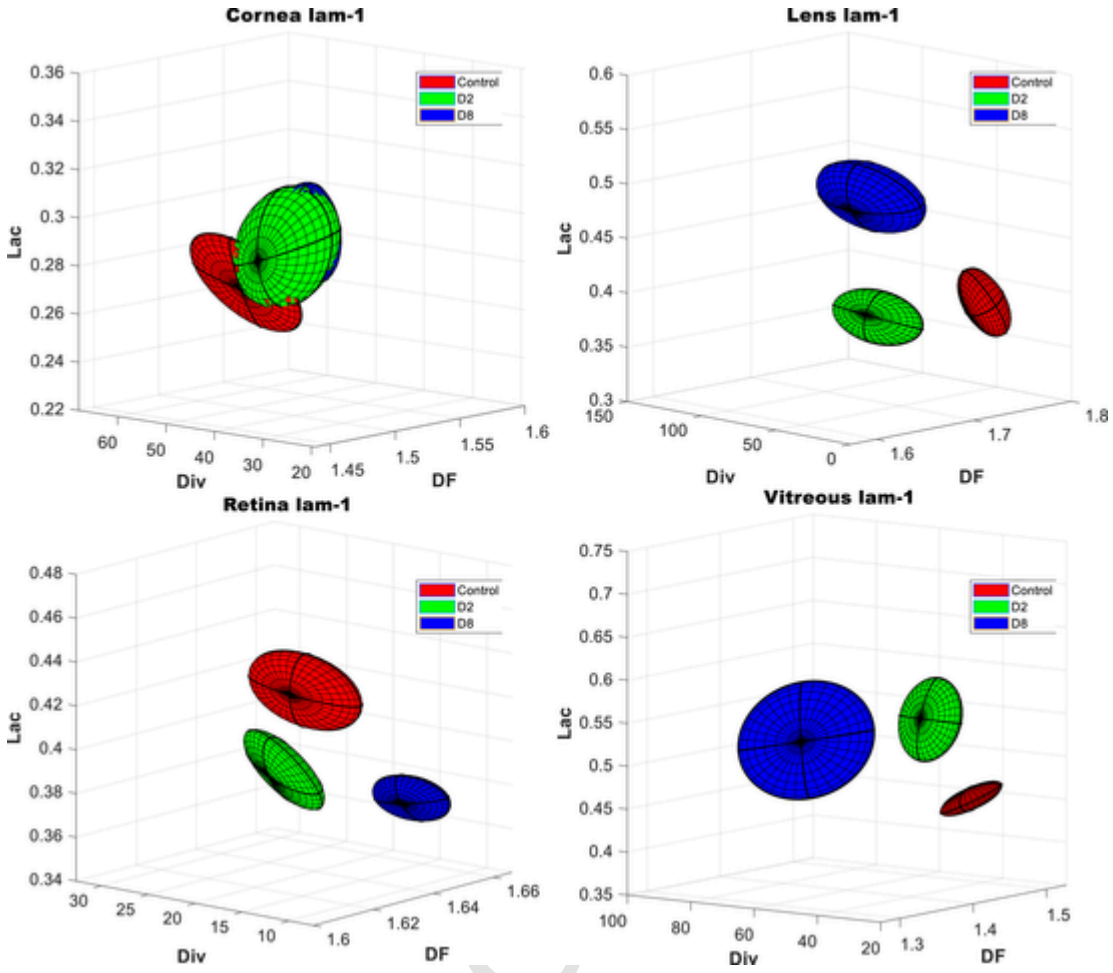

Fig. 10. graphical representation as ellipsoids for the mean´s distribution data, for all the structures stained with anti-laminin-1.

References

[1] O S Al-Kadi Fractals for biomedical texture analysis. Biomedical texture analysis. Academic Press; 2017. p. 131–161.

[2] C Allain, M Cloitre Characterizing the lacunarity of random and deterministic fractal sets. Phys Rev A 1991;44:3552–3558. doi:10.1103/PhysRevA.44.3552.

[3] L D Botto, A Lisi, C Bower, M A Canfield, N Dattani, C Vigan, et al. Trends of selected malformations in relation to folic acid recommendations and fortification: an international assessment. Birth Defects Res 2006;76(10):693-705.

[4] C M Breki, A Dimitrakopoulou-Strauss, J Hassel, T Theoharis, C Sachpekidis, L Y Pan, et al. Fractal and multifractal analysis of PET/CT images of metastatic melanoma before and after treatment with ipilimumab. EJNMMI Res 2016;6(16). doi:10.1186/s13550-016-0216-5.

[5] A Busby, L Abramsky, H Dolk, B Armstrong, Eurocat Folic Acid Working Group Preventing neural tube defects in Europe: population based study. BMJ 2005;330(7491):574 575. doi:10.1136/bmj.330.7491.574.

[6] M R Chernick Bootstrap methods: a guide for practitioners and researchers. Hoboken. Hoboken (New Jersey): John Wiley & Sons. Inc.; 2008.

[7] A Chhabra, R V Jensen Direct determination of the f(alpha) singularity spectrum. Phys Rev Lett 1989;62:1327–1330. doi:10.1103/PhysRevLett.62.1327.

[8] E V L Costa, R A Nogueira Fractal, multifractal and lacunarity analysis applied in retinal regions of diabetic patients with and without nonproliferative diabetic retinopathy. Fractal Geom Nonlinear Anal Med Biol 2015;1:112–119.

[9] M Cui, L Xu, H Wang, S Ju, S Xu, R Jing Combining Nordtest method and bootstrap resampling for measurement uncertainty estimation of hematology analytes in a medical laboratory. Clin. Biochem 2017;50:1067–1072.

[10] A Depeursinge, O S Al-Kadi, J R Mitchell Biomedical texture analysis: fundamentals, tools and challenges. London-United Kingdom: Academic Press; 2017.

[11] Y Ding, H Dai, H Zhang Automatic detection of microcalcifications with multi-fractal spectrum. Biomed Mater Eng 2014;24:3049–3054.

[12] M Donald Multivariate statistical methods. New York: McGraw Hill; 1990.

[13] P L Dong Lacunarity analysis of raster datasets and 1D, 2D, and 3D point patterns. Comput Geosci 2009;35:2100–2110. doi:10.1016/j.cageo.2009.04.001.

[14] G Dougherty, G M Henebry Fractal signature and lacunarity in the measurement of the texture of trabecular bone in clinical CT images. Med Eng Phys 2001;23:369–380. doi:10.1016/s1350-4533(01)00057-1.

[15] B Efron, R J Tibshirani An introduction to the bootstrap: monographs on statistics and applied probability, 57. New York and London: Chapman and Hall/CRC.; 1993.

[16] J Feder Fractals plenum. New York: Press; 1988.

[17] D L Goodhue, W Lewis, R Thompson Does PLS have advantages for small sample size or non-normal data? MIS Q. Appl Probab 2012;57:981–1001. New York and London: Chapman and Hall/CRC.

[18] E Hadzieva, D C Bogatinoska, L Gjergjeska, M Shuminoska, R Petroski Review of the software packages for estimation of the fractal dimension. ICT Innov 2015;201–211.

[19] T C Halsey, M H Jensen, L P Kadanoff, I Procaccia, B I Shraiman Fractal measures and their singularities: the characterization of strange sets. Phys Rev A 1986;33:1141.

[20] S Havlin, S V Buldyrev, A L Goldberger, R N Mantegna, S M Ossadnik, C K Peng, et al. Fractals in biology and medicine. Chaos Solitons Fractals 1995;6:171–201.

[21] G M Henebry, H J H Kux Lacunarity as a texture measure for SAR imagery. Int J Remote Sens 1995;16:565–571.

[22] M-G Hu, J-F Wang, Y Ge Super-resolution reconstruction of remote sensing images using multifractal analysis. Sensors 2009;9:8669.

[23] John E Hutchinson Fractals and self similarity. Indiana Univ Math J 1981;30:713–747.

[24] A Karperien FracLac for imagej. Charles Sturt University; 2013.

[25] Karperien, A. (2016, July 12). Email interview.

[26] G Landini Fractals in microscopy. J Microsc 2011;241:1–8. doi:10.1111/j.1365-2818.2010.03454.x.

[27] Legland, D., 2019. Geom3d. [On-line]. Available on: http://www.mathworks.com/matlabcentral/fileexchange/24484-geom3d.[RetrievedMarch19,2019].

[28] A-H Li, P P Liu, F J Villarreal, R A Garcia Dynamic changes in myocardial matrix and relevance to disease: translational perspectives. Circ Res 2014;114:916–927.

[29] P Liatsis Recent trends in multimedia information processing. Proceedings of the 9th international workshop on systems, signals and image processing, Manchester Town Hall, UK. World Scientific; 2002.

[30] S Liu, X Fan, C Zhang, Z Wang, S Li, Y Wang, et al. MR imaging based fractal analysis for differentiating primary CNS lymphoma and glioblastoma. Eur Radiol 2019;29(3):1348–1354.
[31] R Lopes, N Betrouni Fractal and multifractal analysis: a review. Med Image Anal 2009;13:634–649. doi:10.1016/j.media.2009.05.003.
[32] P Lu, K Takai, V M Weaver, Z Werb Extracellular matrix degradation and remodeling in development and disease. Cold Spring Harb Perspect Biol 2011;3:a005058.
[33] P Mahalanobis Mahalanobis distance. Proc Natl Inst Sci India 1936;49:234–256.
[34] E Maldonado, J Murillo, C Barrio, A del Rio, J Perez-Miguelsanz, Y Lopez-Gordillo, et al. Occurrence of cleft-palate and alteration of Tgf-beta(3) expression and the mechanisms leading to palatal fusion in mice following dietary folic-acid deficiency. Cells Tissues Organs 2011;194:406–420.
[35] B B Mandelbrot The fractal geometry of nature. New York: WH freeman; 1983.
[36] R E Plotnick, R H Gardner, R V Oneill Lacunarity indexes as measures of landscape texture. Landsc Ecol 1993;8:201–211. doi:10.1007/bf00125351.
[37] N Popovic, M Radunovic, J Badnjar, T Popovic Fractal dimension and lacunarity analysis of retinal microvascular morphology in hypertension and diabetes. Microvasc Res 2018;118:36–43.
[38] A N Posadas, D Giménez, R Quiroz, R Protz Multifractal characterization of soil pore systems. Soil Sci Soc Am J 2003;67:1361–1369.
[39] W Rasband ImageJ. Bethesda, Maryland, USA: US National Institutes of Health; 1997. http.imagej.nih.gov/ij 2012.
[40] A Roy, E Perfect, W M Dunne, L D McKay A technique for revealing scale-dependent patterns in fracture spacing data. J Geophys Res: Solid Earth 2014;119:5979–5986.
[41] D A Russell, J D Hanson, E Ott Dimension of strange attractors. Phys Rev Lett 1980;45:1175.
[42] H Salat, R Murcio, E Arcaute Multifractal methodology. Phys A – Stat Mech Appl 2017;473:467–487. doi:10.1016/j.physa.2017.01.041.
[43] D S Santos, L C B Santos, A A T Carvalho, J C Leao, C Delrieux, T Stosic, et al. Multifractal spectrum and lacunarity as measures of complexity of osseointegration. Clin Oral Investig 2016;6:1271–1278.
[44] S Siegel Nonparametric statistics for the behavioral sciences. New York: McGraw-hill; 1956.
[45] O Sijilmassi, J M López-Alonso, M C Barrio Asensio, A Del Río Sevilla Alteration of lens and retina textures from mice embryos with folic acid deficiency: image processing analysis. Graefe's Arch Clin Exp Ophthalmol 2018;1–13. doi:10.1007/s00417-018-4176-5.
[46] O Sijilmassi, J M López-Alonso, M C Barrio Asensio, A Del Río Sevilla Collagen IV and laminin-1 expression in embryonic mouse lens using principal components analysis technique. J Microsc 2018;271:207–221. doi:10.1111/jmi.12709.
[47] O Sijilmassi, J M López-Alonso, A Del Río Sevilla, J Murillo González, M C Barrio Asensio Biometric alterations of mouse embryonic eye structures due to short-term folic acid deficiency. Curr Eye Res 2018;1–8. doi:10.1080/02713683.2018.1545911.
[48] T Smith Jr., G Lange, W Marks Fractal methods and results in cellular morphology—dimensions, lacunarity and multifractals. J Neurosci Methods 1996;69:123–136.
[49] A Szczepaniak, W Macek Asymmetric multifractal model for solar wind intermittent turbulence. Nonlinear Process Geophys 2008;15:615–620.
[50] V Talaulikar, S Arulkumaran Folic acid in pregnancy. Obstet Gynaecol Reprod Med 2013;23:286–288.
[51] The MathWorks Inc. MATLAB – the Language of technical computing, version R2015a (8.5). Massachusetts: Natick; 2015. URL http://http://www.mathworks.com/products/matlab/.
[52] R D Urda-Benitez, A E Castro-Ospina, A Orozco-Duque Feature extraction based on time-singularity multifractal spectrum distribution in intracardiac atrial fibrillation signals. Tecno Lógicas 2017;20:97–111.
[53] J X Xi, W Z Zhao, J E Yuan, J Kim, X H Si, X W Xu Detecting lung diseases from exhaled aerosols: non-invasive lung diagnosis using fractal analysis and SVM classification. PLoS One 2015;10(19). doi:10.1371/journal.pone.0139511.
[54] P Waliszewski The quantitative criteria based on the fractal dimensions, entropy, and lacunarity for the spatial distribution of cancer cell nuclei enable identification of low or high aggressive prostate carcinomas. Front Physiol 2016;7:34. doi:10.3389/fphys.2016.00034. doi.org/.